NANO LETTERS

Letter

pubs.acs.org/NanoLett

# Coupling Localized Plasmonic and Photonic Modes Tailors and Boosts Ultrafast Light Modulation by Gold Nanoparticles

Xiaoli Wang,[†,§] Roberta Morea,[‡] Jose Gonzalo,[‡] and Bruno Palpant*[,†]

[†]Laboratoire de Photonique Quantique et Moléculaire, UMR 8537—CNRS, Ecole Normale Supérieure de Cachan, CentraleSupélec, Grande Voie des Vignes, 92295 Châtenay-Malabry CEDEX, France

[§]Laboratory of Nanomaterials, National Center for Nanoscience and Technology, Beiyitiao No. 11, Zhongguancun, Beijing 100190, P. R. China

[‡]Laser Processing Group, Instituto de Óptica, CSIC, Serrano 121, 28006 Madrid, Spain

*S* *Supporting Information*

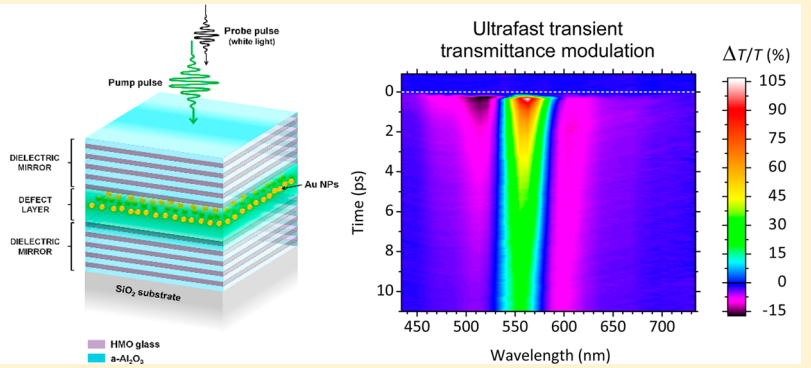


**ABSTRACT:** Plasmonic nanoparticles offer a broad range of functionalities, owing to their ability to amplify light in the near-field or convert it into heat. However, their ultrafast nonlinear optical response remains too low to envisage all-optical high-rate photonic processing applications. Here, we tackle this challenge by coupling the localized plasmon mode in gold nanoparticles with a localized photonic mode in a 1D resonant cavity. Despite the nonradiative losses, we demonstrate that a strong, reversible, and ultrafast optical modulation can be achieved. By using a light pumping fluence of less than 1 mJ $cm^{-2}$, a change of signal transmittance of more than 100% is generated within a few picosecond time scale. The nanoparticle transient optical response is enhanced by a factor of 30 to 40 while its spectral profile is strongly sharpened. The large nonlinear response of such plasmonic cavities could open new opportunities for ultrafast light processing at the nanoscale.

**KEYWORDS:** *plasmonics, photonic cavity, ultrafast modulation, transient optical response, nonlinear optical response, gold nanoparticles*

Localized surface plasmon resonances (LSPRs) in noble metal nanoparticles have recently triggered many thrilling developments.[1−10] Remarkable optical properties result from the excitation of these resonance modes in the stationary regime. Beyond that, the transient behavior also appears worth exploring as the nanoparticle optical response can be modified within a very short time scale following the absorption of a light pulse.[11] This could bestow to metal nanoparticles the ability to modulate light for integrated optics applications. However, the optically driven modifications are not significant enough for reasonable control energies and require the excitation of plasmon-polaritons rather than LSPRs,[12−15] the involvement of other photoactive components,[16−19] or the excitation of larger plasmonic metamaterials.[20] Nonlocality was also exploited in long gold nanorods to obtain a significant ultrafast nonlinear response[21] that was recently theoretically proposed for silicon integrated photonic processing.[22] Besides, waveguide photonic modulation using plasmonic nanostructures as coherent perfect absorbers was theoretically suggested.[23]

Introducing metal films[24] or metal nanoparticles[25] in 1D photonic crystals has been shown to result in significant third-order nonlinear optical response enhancement. Similarly, combining metal nano-objects with resonant electromagnetic cavities for coupling localized plasmonic and photonic modes is an appealing principle to obtain new optical functions,[26−34] provided the nonradiative losses associated with the LSPR do not dampen the cavity resonance too much. It was also recently demonstrated that the optical absorptance of a layer of gold nanoparticles can be enhanced and spectrally shaped by conditioning the nanoparticles in a 1D photonic crystal cavity.[35,36] While these developments played with the

**Received:** January 20, 2015
**Revised:** March 17, 2015





DOI: 10.1021/acs.nanolett.5b00226
*Nano Lett.* XXXX, XXX, XXX−XXX

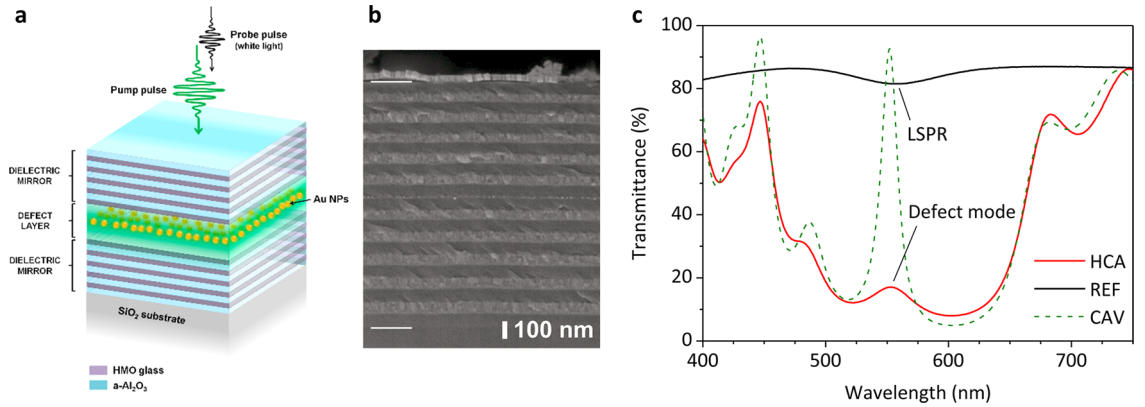


**Figure 1.** Hybrid plasmonic–photonic cavity and its optical properties in the stationary regime. (a) Schematic view of the hybrid cavity. The half-wave defect layer ($a$-$Al_2O_3$) is conditioned between two dielectric mirrors consisting of alternate stacks of high (HMO glass) and low ($a$-$Al_2O_3$) refractive index quarter-wave films. A monolayer of spherical gold nanoparticles embedded in $a$-$Al_2O_3$ is set at the middle of the cavity. The multilayer device lies on a fused silica substrate. A 200 fs pump laser pulse tuned at the localized surface plasmon resonance of the nanoparticles is sent onto the device. The subsequent ultrafast transient changes of the optical properties of the nanoparticles are then probed by a white-light supercontinuum laser pulse. The dynamics of the process is recovered by varying the pump–probe delay. (b) Cross-sectional scanning electron microscopy (SEM) image of the hybrid cavity HCA produced on $SiO_2$. Dark and light layers correspond to $a$-$Al_2O_3$ and HMO, respectively. The layer containing Au nanoparticles can be appreciated at the center of the defect layer. Horizontal white lines indicate the substrate–film and the film-Au coating interfaces. (c) Stationary optical transmittance of the hybrid cavity HCA (red) at normal incidence. The defect mode can be identified in the photonic band gap. The data for the reference layer of $a$-$Al_2O_3$-embedded gold nanoparticles (REF) is included (black line), as well as the calculated transmittance of the bare cavity with no nanoparticle (CAV, green dashed line).

plasmonic–photonic coupling in the stationary regime, we theoretically demonstrated in a previous work that they could be exploited in the transient regime to strongly amplify the ultrafast nonlinear response of gold nanoparticles and achieve a large ultrafast optical modulation.[37] Here, we use an improved scheme of the working principle to demonstrate experimentally this process in a 1D hybrid cavity, along with the model that allows a reliable description of its ultrafast properties.

**Design and Stationary Optical Response of the 1D Hybrid Cavity.** Our approach relies on two principles. First, we aim at using the coupling to maximize the electromagnetic energy input in the nanoparticles. As the electric field amplitude associated with the defect mode of a resonant cavity is maximum at its center, the best configuration is to locate nanoparticles in this region rather than spread them in the whole defect layer.[36,37] Additionally, the design wavelength of the hybrid cavity (HC), that is, the wavelength of the defect mode at normal incidence, should match the spectral domain of the LSPR where the absorption coefficient of the nanoparticles is the highest. This is similar to the requirement for enhancing the light absorption in the stationary regime.[28,35,36] Second, the induced modification of the nanoparticle optical properties must result in the maximum modification of the device transmittance, which occurs when the plasmon resonance matches the defect mode wavelength.[37] Based on these principles, we have designed HCs as shown in Figure 1a: a defect layer consisting of a thin monolayer of Au nanoparticles is sandwiched between two layers of amorphous aluminum oxide ($a$-$Al_2O_3$). This defect layer is set between two dielectric mirrors, each of them consisting of a stack of five bilayers of quarter-wave films of high (H) and low (L) refractive index dielectric materials. Hence, the global Au concentration in the HC remains low, although the local nanoparticle density in the central layer is high. This enables the nanoparticles to experience the highest field in the cavity while keeping the overall light absorption sufficiently weak to preserve the field enhancement effect. This multilayer photonic device was produced by alternate pulsed laser deposition (a-PLD), suited for the fabrication of nanocomposite layers[38,39] (see Figure 1b and Supporting Information for details regarding sample elaboration and characterization). The optical properties of the cavity were calculated by using a multilayer optical model based on the transfer matrix method.[40] The dielectric function of the central defect layer was modeled by the Yamaguchi effective medium theory, well suited for dense monolayers of nanospheres.[41,42] The optical indices of the different L and H layers were deduced from ellipsometric measurement data (see Supporting Information for further details). The design wavelength of the hybrid cavity (named HCA) was set at 553 nm, which allows an exact match of the plasmon resonance and the defect mode, both peaking at 549 nm at the incidence angle of the pump beam in the experiments. From the values of the refractive index of the different dielectric films, the thicknesses of the quarter-wave layers in the mirrors were calculated to get the desired design wavelength. Finally, the nominal thickness of the defect layer was chosen to match the conditions for exciting the first resonance mode of the cavity.

The optical response of the HCA in the stationary regime exhibits characteristics stemming from both the cavity and the nanoparticles. Figure 1c shows the transmittance of the HCA together with that of the bare nanocomposite defect layer (REF, see Supporting Information). The calculated transmittance of a bare cavity (CAV), identical to HCA except from the replacement of the central composite layer by a pure $a$-$Al_2O_3$ layer having the same thickness, is also reported in Figure 1c. For REF, the plasmon band appears in the transmittance spectrum as a slight trough at 557 nm, which corresponds to a maximum of absorptance at 549 nm when accounting for the reflectance. For the cavity HCA, the photonic band gap can be observed between ~450 and ~650 nm, with the defect mode at 553 nm at normal incidence. Since nanoparticles efficiently absorb light at the LSPR, this mode is significantly quenched and broadened as compared with what is obtained in usual photonic cavities. From the transmittance and reflectance


DOI: 10.1021/acs.nanolett.5b00226
Nano Lett. XXXX, XXX, XXX–XXX

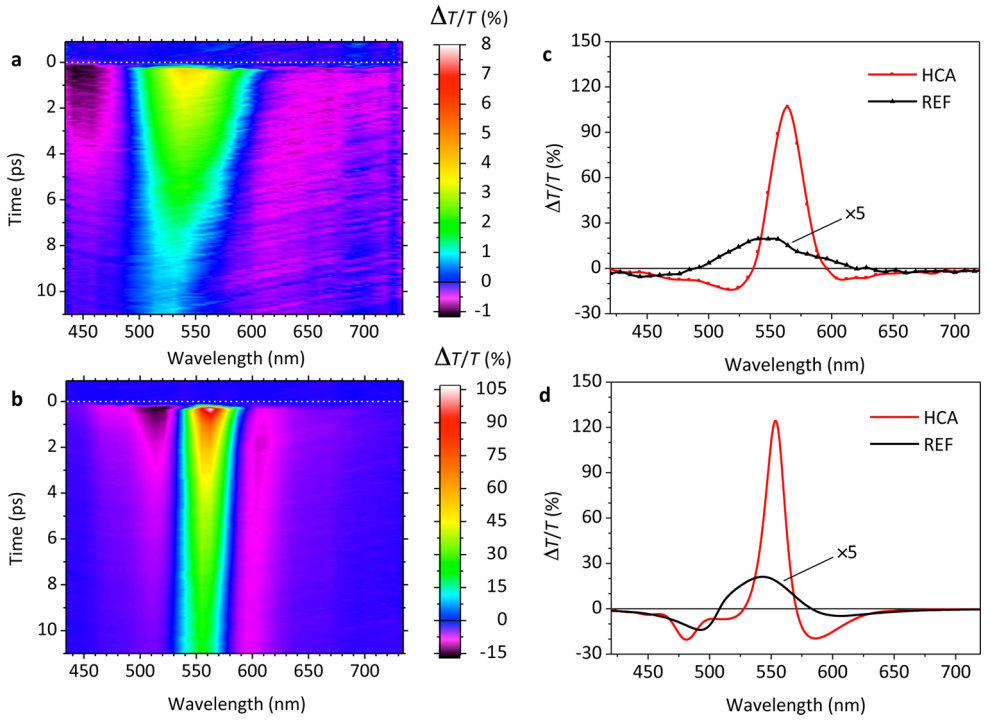


**Figure 2.** Ultrafast photoinduced modulation of the optical transmittance. (a) Spectral and temporal dependence of the transient transmittance of the reference layer of alumina-embedded gold nanoparticles (REF), as measured by pump−probe broadband spectroscopy over the visible range for 12 ps. (b) Transient transmittance map of the hybrid plasmonic−photonic cavity HCA displayed with the same time and wavelength scales as in panel a. In both panels a and b, time zero corresponds to the excitation by the 200 fs pump laser pulse, the fluence and wavelength of which are 0.9 mJ $cm^{-2}$ and 550 nm, respectively. The color level scales are different but the ratio of negative minimum and positive maximum is maintained for sake of comparison. (c) Experimental spectra of the transient transmittance relative variations for sample REF (black) and HCA (red) at their maximum, that is, just after optical pumping. The curve for sample REF has been 5-fold magnified for sake of clarity. (d) Equivalent spectra as simulated by using the model accounting for the athermal distribution of the conduction electrons. No fitting procedure was used for these calculations. The irradiation conditions for both panels c and d are the same as those of panels a and b.

spectra, we find that the absorption peak of HCA is four times higher and more than twice sharper than the one of the bare nanocomposite REF film. This effect, already observed in previous works,[36] stems from the fact that the nanoparticles in the middle of the HC undergo an electromagnetic field with higher amplitude than in the REF film (i.e., without the two mirrors). Consequently, the quantity of energy dissipated in metal nanoparticles is higher in the cavity for the same incident light power (but remains low enough to avoid photothermally induced local damages to the sample). Furthermore, this effect is conditioned by the spectral profile of the defect mode, which explains the spectral shaping of the apparent LSPR absorption band.

**Ultrafast Nonlinear Optical Response of the Hybrid Cavity.** The ultrafast transient optical response of HCA was measured by pump−probe laser spectroscopy, the basic principle of which is described in Figure 1a (see Supporting Information for more details). The pump-induced transmittance relative modulation $\Delta T/T = (T_{ON} - T_{OFF})/T_{OFF}$, where $T_{OFF}$ is the stationary sample transmittance and $T_{ON}$ the transmittance after the pump pulse, is monitored as a function of the pump−probe delay time. The pump wavelength is 550 nm, the pulsewidth is 200 fs and the incident peak power density is 4.2 GW $cm^{-2}$, which corresponds to a fluence of 0.9 mJ $cm^{-2}$. The probe beam is a white-light supercontinuum (425−750 nm) of 150 fs pulses. The resulting transient response for REF and HCA are displayed in Figure 2a and b, respectively. In both cases, the transient transmittance signal steeply rises following the pump pulse, reaches a maximum within a subpicosecond time scale and then relaxes back to equilibrium within a few picoseconds. In order to highlight the maximum transmittance modulation, a snapshot of the bare film (REF) and hybrid cavity (HCA) transient spectra probed just after pumping are displayed in Figure 2c. The data for REF sample (Figure 2a and c) reveal the "plasmon bleaching" behavior usual for noble metal nanospheres, that is, the photoinduced increase of the transmittance at the LSPR and the photoinduced absorption in its red and blue wings,[11,43] which mainly stems from the *Fermi smearing* mechanism that follows the pump pulse.[44,45] The initial fast and high pump energy input in the conduction electron gas modifies the distribution of these conduction electrons around the Fermi level. Due to Pauli principle, this causes the ultrafast modulation of interband transition probabilities in a spectral region ranging from about $-h\nu_{pump}$ to $+h\nu_{pump}$ around the interband transition threshold ($h\nu_{pump}$ is the pump photon energy). The resulting modification of the metal dielectric function is then amplified by the local field enhancement associated with the LSPR activated by the probe.[45] It can be noticed that for REF sample the signal extends over a large spectral range. This spectral profile is strongly affected once the nanoparticle layer is conditioned in the photonic cavity, as revealed by Figure 2b and c. While the plasmon bleaching is still observed, the coupling of the localized plasmon mode with the resonant mode of the cavity results in the sharpening and spectral shift of the transient response. In other words, the defect mode of the cavity filters and enhances the transient


DOI: 10.1021/acs.nanolett.5b00226
*Nano Lett.* XXXX, XXX, XXX−XXX

response of the nanoparticle layer within a narrow spectral range.

The main difference observed when comparing the transient behavior of the two samples under the same irradiation conditions is the large enhancement of the signal modulation once the nanoparticle layer is conditioned in the cavity. The positive transient peak is about 30 times higher than for REF. This factor increases up to 40 for other irradiation conditions. Under a fluence of only 0.9 mJ $cm^{-2}$ the transmittance of light through the hybrid device at normal incidence experiences a magnitude modulation of 107%, which is larger than the 80% that was obtained earlier with aligned gold nanorods irradiated at a much higher fluence (7.5 mJ $cm^{-2}$) and needing a 40° probe incidence angle.[8] In that case, the high transient signal was ascribed to the involvement of nonlocality in the contribution of the longitudinal LSPR to the optical response.

Let us now analyze deeper the physical origin of the enhancement and sharpening of the nonlinear response in HCA. The resonant cavity effect first increases the pump field amplitude experienced by the nanoparticles, which modifies the optical properties of the whole defect layer. This affects mainly its absorptive component as, contrarily to its linear refractive index, the only contribution to its global linear absorption is the one of nanoparticles.[37] The consequence is a strong pump-induced modulation of the magnitude of the cavity defect mode. In addition, the latter undergoes a slight detuning (i.e., spectral shift), which can be deduced from the fact that the differential signal $\Delta T/T$ is not perfectly symmetric relative to the stationary position of the mode peak at 553 nm (see Figure 2c, and Figure S5 of the Supporting Information). This slight transient detuning of the defect mode is not due to a pump-induced variation of the thickness of the defect layer (see section 5.b of the Supporting Information), or of its refractive index, but rather to the spectral dispersion of the variation of its absorption coefficient in this spectral domain.[37] The pump-induced changes transiently modify the filtering property of the cavity, which are then experienced by the probe signal. To further assess this statement, we have simulated the properties of the bare nanocomposite layer (REF sample), subsequently filtered by the cavity containing no nanoparticle (CAV sample). This configuration is equivalent to HCA in which the nanoparticles would have been moved outside the cavity. We observe obvious differences with the properties of HCA, not only in the linear transmittance but also in the magnitude and spectral profile of the ultrafast nonlinear response (see Supporting Information for details). This further demonstrates that the role of the cavity—disregarding its enhancement effect—does not amount to a simple stationary filtering; rather, the plasmonic−photonic coupling results in a dynamic modulation of the cavity spectral filtering properties.

$\Delta T/T$ is well suited to characterize the effectiveness of the device to modulate a light signal. However, the value of $\Delta T/T$ could be artificially increased by decreasing the linear transmittance $T$. For instance, the performances of HCA could be achieved by simply using a bare nanocomposite layer with a quantity of metal 30 times larger than in REF, or by stacking 30 successive REF layers. Let us, however, underline that the signal intensity would be severely degraded due to the dramatic decrease of $T$, and that the relaxation would be slower than with HCA, as will be shown later. In order to assess the effectiveness of the photonic−plasmonic coupling itself on the HCA ultrafast transient response independently of the quantity of nanoparticles used, the relative change of the optical density upon pump pulse irradiation, $\Delta OD/OD$, can be alternately used. We have then determined the optical density ($OD = -\log_{10} T$) and its relative variation [$\Delta OD/OD = -\log_{10}(\Delta T/T + 1)$] from our experimental data (see Supporting Information). The maximum value of $|\Delta OD/OD|$ reaches 0.38 at 0.8 ps for HCA, which is two times higher than for REF. In addition, the coupling leads to an obvious sharpening of the modulation spectral profile around its maximum. These results underline the relevance of coupling localized photonic modes with plasmon modes to enhance the ultrafast photoinduced modulation of light by metal nanoparticles.

In order to analyze the nonlinear response of our HC at its maximum, which is reached just after the excitation by the pump pulse, we built a model suited for this short time range (see Supporting Information for details). Within the very first picoseconds, the conduction electron distribution in the metal is put out of equilibrium. Its time and energy dependence in this athermal regime can be well described by the Boltzmann equation. This rate equation accounts for the instantaneous electron distribution modification under absorption of incident light energy, electron−electron, and electron−phonon scattering processes. The heat release toward the surrounding host medium plays a negligible role within this short time domain.[46] We solved the Boltzmann equation by using the relaxation time approximation in the framework of the Landau theory of Fermi liquids.[47] The change of the electron distribution results in the modification of interband transitions in the vicinity of the LSPR spectral domain, and then in the time evolution of the dielectric function of gold,[44,45] which is calculated through Lindhard's theory by using Rosei's model for the energy band structure.[47] The time-dependent dielectric function of gold is then used in the multilayer model as already described above for the stationary optical properties of the cavity. Once the multilayer morphology has been fixed, the only input parameter of our model is the time profile of the instantaneous power absorbed by the nanoparticles, which follows the pump pulse. From the experimental absorptance, the surface coverage and the thickness of the nanoparticle layer, the pump peak power absorbed per metal volume unit for an incident peak power of 4.2 GW $cm^{-2}$ is calculated to be $4.0 \times 10^{21}$ W $m^{-3}$ for REF and $16.6 \times 10^{21}$ W $m^{-3}$ for HCA samples, respectively. The results are displayed in Figure 2d. They show very good agreement with the experimental data (Figure 2c): The spectral profile is similar and reproduces very well the magnitude of the modulation. The fact that the features observed appear to be slightly broader in the experimental curves, for both HCA and REF, is ascribed to the effect of the nanoparticle size and shape distributions on the transient response, which are not considered by the model. The only noticeable discrepancy concerns the spectral position of the predicted plasmon bleaching feature for HCA, shifted of about 10 nm to the blue as compared with the experimental data and the precise origin of which is unclear. The larger energy input in the metal nanoparticles due to the cavity effect for HCA may depart the actual behavior from the relaxation time approximation used to solve Boltzmann equation. In addition, the simulation predicts a local minimum of the transmittance modulation at 480 nm, which is not observed in the experimental results. This can be correlated to the overestimation, in the stationary regime, of the magnitude of a small peak appearing in the sharp blue edge of the photonic bandgap at this wavelength (see Supporting Information, Figure S3b) and, thus, is independent of the transient response modeling. Nevertheless, the good agreement


DOI: 10.1021/acs.nanolett.5b00226
Nano Lett. XXXX, XXX, XXX−XXX

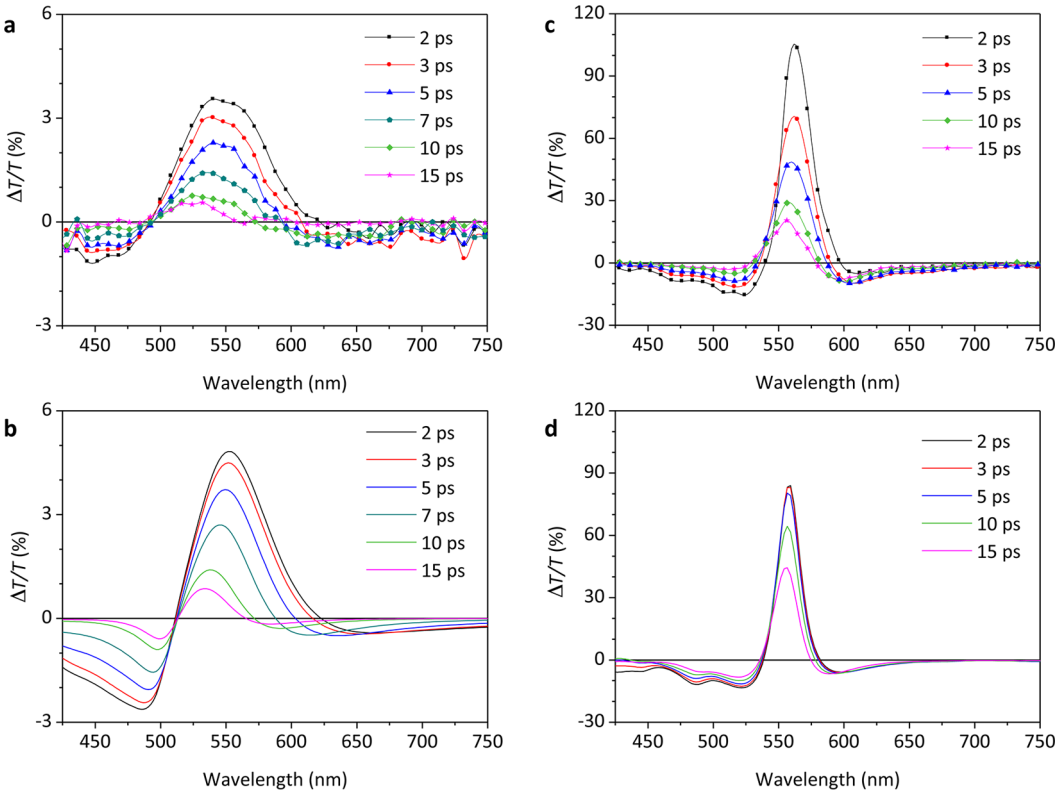


**Figure 3.** Time evolution of the transmittance modulation spectra. Spectral profile of the transient differential transmittance at different time delays within the range 2−15 ps. (a,b) Reference layer of alumina-embedded gold nanoparticles (REF). (c,d) Photonic crystal hybrid cavity (HCA). (a,c) Results of pump−probe spectroscopy measurements carried out with the same incident laser intensity (peak value $I_0$ = 4.2 GW cm$^{-2}$). (b,d) Results of numerical simulations obtained by using the three-temperature model with the same incident intensity as in the experiments.

of our model calculations with the experimental results confirms that the maximum transmittance modulation of the device is reached during the athermal regime and originates mainly from the ultrafast modification of the interband transition contribution to the dielectric function of gold close to their threshold. The fast increase of the electron−electron scattering rate due to the high internal energy rise within the electron gas has sometimes been invoked to explain the plasmon bleaching transient behavior.[43,48,49] Although this effect contributes certainly to the ultrafast response, we nevertheless demonstrate that its contribution remains negligible compared to that of the pump-induced interband transition modification in the LSPR spectral range.

**Relaxation Dynamics.** The dynamics of the transient optical response is also affected by the coupling. Figure 2 compares the time evolution of the huge transient signal observed in HCA with that in REF. Once the maximum is reached after a very short time, the transient signal relaxes back to equilibrium. The transient relaxation of the nanoparticle optical response exhibits two components after completion of the athermal regime: (1) A fast component with a characteristic time of a few picoseconds, which corresponds to the electron−phonon energy exchange[50] and (2) a slow one which is related to the heat release through the interface toward the surrounding medium and lasts for a few hundreds of picoseconds.[51] After 11 ps, a still significant signal tail persists in HCA. This corresponds to the slow component of the relaxation, related to nanoparticle cooling: As the energy input in HCA is larger than in REF, the heat to be released before reaching thermal equilibrium is also larger, which explains this persistent detectable signal. In addition, a slight blue shift of the induced transmittance peak is observed along the relaxation, which is more pronounced when the nanoparticle layer is not conditioned in a cavity. In order to examine deeper the relaxation process, the transmittance modulation measured at different pump−probe delays after the completion of the athermal regime is displayed in Figure 3 for sample REF (a) and the cavity HCA (c). Calculations based on the three-temperature model[52,53] were carried out in this time range. Assuming now that the conduction electron gas is at internal thermal equilibrium, this approach considers the influence of the time-dependent electron−electron and electron−phonon scattering rates on the contribution of intraband transitions,[54] as well as the heat release to the surrounding medium, whereas these effects were negligible in the ultrashort time domain.[45,55,56]

Simulations shown in Figure 3b reproduce well the time evolution of the spectral position and the amplitude of the transient transmittance measured for the bare nanocomposite REF sample. The blue shift of both the maximum and the zero-crossing point observed along the relaxation, as well as the weak red shift of the low-wavelength minimum, originate from a nonuniform relaxation time, which increases as photon energy gets closer to the interband transition threshold (located at about 510 nm). Indeed, the interband transition probability is ruled by the electron distribution $f(E)$ in the final state, that is, in the conduction band close to the Fermi level $E_F$ ($E$ is the electron energy). Once the thermal regime is reached, the Fermi−Dirac distribution evolves, during the cooling, with a relative instantaneous variation $|df(E, t)/f|$, which uniformly


DOI: 10.1021/acs.nanolett.5b00226
Nano Lett. XXXX, XXX, XXX−XXX

increases with $|E-E_F|$. In the case of HCA (Figure 3c) the shift is strongly attenuated compared with REF, and the decay is faster. This stems from the filtering by the cavity which limits the signal within a restricted spectral domain imposed by the defect mode. The blue-shifting and decaying modulation (as in REF) once constrained by a fixed band-pass filter (in HCA) then results in a weaker shift and a faster decay. However, this last point should be counterbalanced by the increase of the electron gas heat capacity with increasing input power, as it has already been shown in the literature.[50,57] As nanoparticles in HCA absorb more energy than in REF due to the cavity, the initial cooling should be slower; this corresponds to the three-temperature model simulations (see Figure 3b and d). However, as these simulations reproduce well the spectral signature of the transient signal in HCA but not its time dependence, whereas both are well depicted for REF, it is likely that the assumptions of the model may be partly invalid for high powers. The strong perturbation of the conduction electron gas distribution, the effects of which on the optical response are amplified and filtered by the coupling of the plasmon mode with the cavity mode, may be involved in this discrepancy. Further investigations are needed to assess precisely the origin of the fast decay in HCA. The measured decay time (delay needed to reach $1/e$ times the maximum modulation) is only 3.4 ps for HCA, whereas it is about 6.0 ps for REF. The very short recovery time of the transient signal in the hybrid cavity imparts a significant advantage for ultrafast photonic applications in the terahertz range.

**Defect Mode Tuning.** Finally, the ultrafast transient response can be spectrally tuned by playing with the relative spectral positions of the localized photonic and plasmonic modes. As the pump-induced modification of the nanocomposite layer dielectric function is strongly dispersed in the spectral range of the LSPR, tuning the photonic mode may enable the exploration of different responses for the global hybrid device.[37] For this, another hybrid cavity (HCB) was designed with a defect mode at 516 nm by modifying the central layer characteristics (see Supporting Information, Figure S7). In the transient regime, the weaker plasmonic−photonic coupling results in a lower power dissipated in the nanoparticles. For the same pump wavelength (550 nm) and intensity (4.2 GW $cm^{-2}$), this power amounts to the same value as in REF sample. HCB is then well suited to highlight the influence of the coupling on the probe beam only. Indeed, its effect on the pumping amplification is eliminated at this pump wavelength, contrary to what occurs in HCA. We then observe a less intense ultrafast modulation (see Supporting Information Figure S8), which is well confirmed by the model calculations. However, the signal is in general much higher than for REF despite the same input power, and its profile is different, thus proving that the probe-induced plasmonic−photonic coupling generates in itself an enhancement of the transient response. The $1/e$ decay time of the maximum modulation in HCB (at 525 nm) is worth 4.8 ps. This case is then intermediate between the dynamics of HCA and REF. This supports the idea that the fast decay in HCA is related to the influence of the plasmonic−photonic coupling. Besides, the spectral shape of the signal modulation is less symmetric in HCB than in HCA. Thus, playing with the spectral interval between the nanoparticle LSPR and the defect mode may allow for choosing the nature of the photonic modulation, affecting mainly either the amplitude of the defect mode or its spectral location.

**Conclusion.** We have engineered the coupling of localized plasmonic and photonic resonant modes in the ultrafast transient regime. For this, a 1D photonic crystal cavity containing a layer of gold nanoparticles has been designed and elaborated. We have then achieved a very significant amplification of the ultrafast nonlinear optical response of the nanoparticles. Under ultrashort light pulse pumping with relatively low fluence of 0.9 mJ $cm^{-2}$, the hybrid cavity exhibits a transmittance variation larger than 100% with a picosecond dynamics. This performance, together with the stacked-layer structure and the absence of need for oblique signal incidence,[21] makes the principle of ultrafast plasmonic−photonic coupling highly suitable for its application in integrated photonics.

Replacing gold nanospheres by nanorods may further offer new outlooks. First, the symmetry lowering leads to the splitting of the resonance mode, enabling for polarization-controlled effects. Second, increasing the nanorod aspect ratio results in both the red-shift and enhancement of the longitudinal LSPR. This could allow for tuning the ultrafast modulation at a desired wavelength, especially in a spectral region where the linear absorption of the signal is low and the change in absorption coefficient is high. Third, because the nonlinear absorption spectral profile close to the longitudinal LSPR is antisymmetric,[56] playing with the relative location of the defect mode and the longitudinal plasmon mode may allow for choosing the type of ultrafast modulation (negative or positive amplitude variation, or spectral shift of the defect mode). Another exciting development of the transient plasmonic−photonic coupling will be to design 2D cavities containing a single metal nanoparticle, as it was already realized in the stationary regime.[28] By reducing the size of the cavity, this would allow us to strongly lower the pump energy needed[58] and will pave the route for ultrafast optical control in photonic waveguide circuits. Besides, the sharp localization of electromagnetic energy in 2D cavities could be exploited for optically driven high-rate modulation of near-field energy transfer, nonlinear optics, or sensing.

## ■ ASSOCIATED CONTENT

### Supporting Information

Fabrication of the hybrid cavity, morphology, stationary optical properties, ultrafast transient response measurement by broadband pump−probe spectroscopy, pump-induced maximum variation of the defect mode of the hybrid cavity, optical properties of the cavity with nanoparticles moved outside, results for a detuned hybrid cavity, relative change of the cavity optical density. This material is available free of charge via the Internet at http://pubs.acs.org.

## ■ AUTHOR INFORMATION

### Corresponding Author

*E-mail: bruno.palpant@centralesupelec.fr. Phone: +33-14-113-1626.

### Notes

The authors declare no competing financial interest.

## ■ ACKNOWLEDGMENTS

The authors thank E. Charron from Institut des NanoSciences de Paris for reflectance spectroscopy measurement. The work of R.M. and J.G. was supported by the Spanish Ministry of Economy & Competitivity (MAT2009-14282-C02-01,



DOI: 10.1021/acs.nanolett.5b00226
Nano Lett. XXXX, XXX, XXX−XXX

TEC2012-38901-C02-01). R.M. was supported by the Spanish Government through a FPI grant.

## REFERENCES


(1) Kühn, S.; Håkanson, U.; Rogobete, L.; Sandoghdar, V.; Kuehn, S.; Hakanson, U. *Phys. Rev. Lett.* **2006**, *97*, 1−4.
(2) Kim, S. S.-W.; Jin, J.; Kim, Y.-J. Y.; Park, I.-Y. *Nature* **2008**, *453*, 757−760.
(3) Zijlstra, P.; Chon, J. W. M.; Gu, M. *Nature* **2009**, *459*, 410−413.
(4) Cherukuri, P.; Glazer, E. S.; Curley, S. A. *Adv. Drug Delivery Rev.* **2010**, *62*, 339−345.
(5) Atwater, H. A.; Polman, A. *Nat. Mater.* **2010**, *9*, 205−213.
(6) Schuller, J. A.; Barnard, E. S.; Cai, W.; Jun, Y. C.; White, J. S.; Brongersma, M. L. *Nat. Mater.* **2010**, *9*, 193−204.
(7) Linic, S.; Christopher, P.; Ingram, D. B. *Nat. Mater.* **2011**, *10*, 911−921.
(8) Ma, H.; Bendix, P.; Oddershede, L. *Nano Lett.* **2012**, *12*, 3954−3960.
(9) Warren, S. C.; Walker, D. a; Grzybowski, B. A. *Langmuir* **2012**, *28*, 9093−9102.
(10) Tame, M. S.; McEnery, K. R.; Özdemir, Ş. K.; Lee, J.; Maier, S. A.; Kim, M. S. *Nat. Phys.* **2013**, *9*, 329−340.
(11) Del Fatti, N.; Vallée, F. *Appl. Phys. B: Lasers Opt.* **2001**, *73*, 383−390.
(12) Kevin F, MacDonald; Sámson, Z. L.; Stockman, M. I.; Zheludev, N. I. *Nat. Photonics* **2009**, *3*, 55−58.
(13) Caspers, J. N.; Rotenberg, N.; van Driel, H. M. *Opt. Express* **2010**, *18*, 19761−19769.
(14) Melikyan, A.; Lindenmann, N.; Walheim, S.; Leufke, P. M.; Ulrich, S.; Ye, J.; Vincze, P.; Hahn, H.; Schimmel, T.; Koos, C.; Freude, W.; Leuthold, J. *Opt. Express* **2011**, *19*, 8855−8869.
(15) Pohl, M.; Belotelov, V. I.; Akimov, I. A.; Kasture, S.; Vengurlekar, A. S.; Gopal, A. V.; Zvezdin, A. K.; Yakovlev, D. R.; Bayer, M. *Phys. Rev. B* **2012**, *85*, 081401.
(16) Dintinger, J.; Robel, I.; Kamat, P. V.; Genet, C.; Ebbesen, T. W. *Adv. Mater.* **2006**, *18*, 1645−1648.
(17) Pacifici, D.; Lezec, H. J.; Atwater, H. A. *Nat. Photonics* **2007**, *1*, 402−406.
(18) Wiederrecht, G. P.; Wurtz, G. A.; Bouhelier, A. *Chem. Phys. Lett.* **2008**, *461*, 171−179.
(19) Abb, M.; Albella, P.; Aizpurua, J.; Muskens, O. L. *Nano Lett.* **2011**, *11*, 2457−2463.
(20) Ren, M.; Jia, B.; Ou, J.-Y.; Plum, E.; Zhang, J.; MacDonald, K. F.; Nikolaenko, A. E.; Xu, J.; Gu, M.; Zheludev, N. I. *Adv. Mater.* **2011**, *23*, 5540−5544.
(21) Wurtz, G. A.; Pollard, R.; Hendren, W.; Wiederrecht, G. P.; Gosztola, D. J.; Podolskiy, V. A.; Zayats, A. V. *Nat. Nanotechnol.* **2011**, *6*, 107−111.
(22) Neira, A. D.; Wurtz, G. A.; Ginzburg, P.; Zayats, A. V. *Opt. Express* **2014**, *22*, 10987.
(23) Bruck, R.; Muskens, O. L. *Opt. Express* **2013**, *21*, 27662−27671.
(24) Lepeshkin, N.; Schweinsberg, A.; Piredda, G.; Bennink, R.; Boyd, R. *Phys. Rev. Lett.* **2004**, *93*, 123902.
(25) Husaini, S.; Teng, H.; Menon, V. M. *Appl. Phys. Lett.* **2012**, *101*, 111103.
(26) De Angelis, F.; Patrini, M.; Das, G.; Maksymov, I.; Galli, M.; Businaro, L.; Andreani, L. C.; Fabrizio, E. Di; Di Fabrizio, E. *Nano Lett.* **2008**, *8*, 2321−2327.
(27) Ameling, R.; Langguth, L.; Hentschel, M.; Mesch, M.; Braun, P. V.; Giessen, H. *Appl. Phys. Lett.* **2010**, *97*, 253116.
(28) Barth, M.; Schietinger, S.; Fischer, S.; Becker, J.; Nüsse, N.; Aichele, T.; Löchel, B.; Sönnichsen, C.; Benson, O. *Nano Lett.* **2010**, *10*, 891−895.
(29) Chamanzar, M.; Adibi, A. *Opt. Express* **2011**, *19*, 22292−22304.
(30) He, Y.; Zhou, H.; Jin, Y.; He, S. *Appl. Phys. Lett.* **2011**, *99*, 043113.
(31) Maksymov, I. S. *Phys. Lett. A* **2011**, *375*, 918−921.
(32) Mukherjee, I.; Hajisalem, G.; Gordon, R. *Opt. Express* **2011**, *19*, 22462−22469.
(33) Xiao, Y.-F.; Liu, Y.-C.; Li, B.-B.; Chen, Y.-L.; Li, Y.; Gong, Q. *Phys. Rev. A* **2012**, *85*, 031805.
(34) Schmidt, M. A.; Lei, D. Y.; Wondraczek, L.; Nazabal, V.; Maier, S. A. *Nat. Commun.* **2012**, *3*, 1108.
(35) Sánchez-Sobrado, O.; Lozano, G.; Calvo, M. E.; Sánchez-Iglesias, A.; Liz-Marzán, L. M.; Míguez, H. *Adv. Mater.* **2011**, *23*, 2108−2112.
(36) Jiménez-Solano, A.; López-López, C.; Sánchez-Sobrado, O.; Luque, J. M.; Calvo, M. E.; Fernández-López, C.; Sánchez-Iglesias, A.; Liz-Marzán, L. M.; Míguez, H. *Langmuir* **2012**, *28*, 9161−9167.
(37) Wang, X.; Palpant, B. *Plasmonics* **2013**, *8*, 1647−1653.
(38) Afonso, C. N.; Gonzalo, J.; Serna, R.; Solis, J. In *Recent Advances in laser Processing of Materials*; Perrière, J., Millon, E., Fogarassy, E., Eds.; Elsevier: Amsterdam, 2006.
(39) *Pulsed Laser Deposition of Thin Films. Applications-Led Growth of Functional Materials*; Eason, R., Ed.; Wiley: Weinheim, Germany, 2007.
(40) Born, M.; Wolf, E. *Principles of optics: electromagnetic theory of propagation, interference and diffraction of light*; Pergamon Press: Oxford, 1964.
(41) Yamaguchi, T.; Yoshida, S.; Kinbara, A. *Thin Solid Films* **1974**, *21*, 173−187.
(42) Toudert, J.; Babonneau, D.; Simonot, L.; Camelio, S.; Girardeau, T. *Nanotechnology* **2008**, *19*, 125709.
(43) Perner, M.; Bost, P.; Lemmer, U.; von Plessen, G.; Feldmann, J.; Becker, U.; Mennig, M.; Schmitt, M.; Schmidt, H.; von Plessen, G. *Phys. Rev. Lett.* **1997**, *78*, 2192−2195.
(44) Bigot, J. Y.; Halte, V.; Merle, J. C.; Daunois, A. *Chem. Phys.* **2000**, *251*, 181−203.
(45) Guillet, Y.; Charron, E.; Palpant, B. *Phys. Rev. B* **2009**, *79*, 195432.
(46) Palpant, B. In *Gold nanoparticles for physics, chemistry and biology*; Louis, C., Pluchery, O., Eds.; Imperial College Press: London, 2012; pp 75−102.
(47) Guillet, Y.; Rashidi-Huyeh, M.; Palpant, B. *Phys. Rev. B* **2009**, *79*, 45410.
(48) Hartland, G. V.; Hodak, J. H.; Martini, I. *Phys. Rev. Lett.* **1999**, *82*, 3188.
(49) Perner, M.; von Plessen, G.; Feldmann, J. *Phys. Rev. Lett.* **1999**, *82*, 3189.
(50) Hodak, J.; Martini, I.; Hartland, G. V. *Chem. Phys. Lett.* **1998**, *284*, 135−141.
(51) Hu, M.; Hartland, G. V. *J. Phys. Chem. B* **2002**, *106*, 7029−7033.
(52) Hamanaka, Y.; Kuwabata, J.; Tanahashi, I.; Omi, S.; Nakamura, A. *Phys. Rev. B* **2001**, *63*, 104302.
(53) Palpant, B. In *Thermal Nanosystems and Nanomaterials*; Volz, S., Ed.; Topics in Applied Physics; Springer: Berlin/Heidelberg, 2009; Vol. *118*, pp 127−150.
(54) Voisin, C.; Del Fatti, N.; Christofilos, D.; Vallée, F. *J. Phys. Chem. B* **2001**, *105*, 2264−2280.
(55) Del Fatti, N.; Voisin, C.; Achermann, M.; Tzortzakis, S.; Christofilos, D.; Vallée, F. *Phys. Rev. B* **2000**, *61*, 956−966.
(56) Baida, H.; Mongin, D.; Christofilos, D.; Bachelier, G.; Crut, A.; Maioli, P.; Del Fatti, N.; Vallée, F. *Phys. Rev. Lett.* **2011**, *107*, 057402.
(57) Park, S.; Pelton, M.; Liu, M.; Guyot-Sionnest, P.; Scherer, N. F. *J. Phys. Chem. C* **2007**, *111*, 116−123.
(58) Nozaki, K.; Tanabe, T.; Shinya, A.; Matsuo, S.; Sato, T.; Taniyama, H.; Notomi, M. *Nat. Photonics* **2010**, *4*, 477−483.




DOI: 10.1021/acs.nanolett.5b00226
*Nano Lett.* XXXX, XXX, XXX−XXX